AGN feedback in dwarf galaxies?

Gohar Dashyan, Joseph Silk, Gary A Mamon, Yohan Dubois, Tilman Hartwig

HAL Id: hal-01715195

https://hal.sorbonne-universite.fr/hal-01715195v1

Submitted on 22 Feb 2018

AGN feedback in dwarf galaxies?

Gohar Dashyan,[1][*] Joseph Silk,[1,2,3,4] Gary A. Mamon,[1] Yohan Dubois[1] and Tilman Hartwig[1]

[1]*Institut d'Astrophysique de Paris (UMR 7095: CNRS and UPMC-Sorbonne Universités), 98 bis bd Arago, F-75014 Paris, France*
[2]*Laboratoire AIM-Paris-Saclay, CEA/DSM/IRFU, CNRS, University Paris VII, F-91191 Gif-sur-Yvette, France*
[3]*Department of Physics and Astronomy, The Johns Hopkins University Homewood Campus, Baltimore, MD 21218, USA*
[4]*BIPAC, Department of Physics, University of Oxford, Keble Road, Oxford OX1 3RH, UK*

ABSTRACT

Dwarf galaxy anomalies, such as their abundance and cusp-core problems, remain a prime challenge in our understanding of galaxy formation. The inclusion of baryonic physics could potentially solve these issues, but the efficiency of stellar feedback is still controversial. We analytically explore the possibility of feedback from active galactic nuclei (AGNs) in dwarf galaxies and compare AGN and supernova (SN) feedback. We assume the presence of an intermediate-mass black hole within low-mass galaxies and standard scaling relations between the relevant physical quantities. We model the propagation and properties of the outflow and explore the critical condition for global gas ejection. Performing the same calculation for SNe, we compare the ability of AGNs and SNe to drive gas out of galaxies. We find that a critical halo mass exists below which AGN feedback can remove gas from the host halo and that the critical halo mass for an AGN is greater than the equivalent for SNe in a significant part of the parameter space, suggesting that an AGN could provide an alternative and more successful source of negative feedback than SNe, even in the most massive dwarf galaxies.

Key words: black hole physics – methods: analytical – galaxies: active – galaxies: dwarf – galaxies: evolution – galaxies: luminosity function, mass function.

1 INTRODUCTION

In the cold dark matter (CDM) cosmological model, larger structures form through successive mergers. Therefore, dwarf galaxies ($M_{vir} < 10^{11} M_\odot$) are potentially left-over building blocks of galaxies and provide a test bed for the CDM model, as the smallest probes of cosmological structure formation. The ΛCDM model has proven successful at reproducing the large scale Universe, however, disparities exist between the theory and observations on small scales: the model predicts too many small galaxies (the 'missing satellites' problem; Moore et al. 1999) and cuspy dark matter profiles that are not yet convincingly observed (Oh et al. 2011), and the most massive dwarfs predicted by ΛCDM simulations are rarely observed (the 'too big to fail' problem; Boylan-Kolchin, Bullock & Kaplinghat 2011). Baryonic feedback, especially from supernovae (SNe), is a currently controversial solution to all these difficulties. Ram-pressure stripping, tidal stripping and harassment are additional mechanisms that should occur in the group environment. It is, however, still unclear whether these mechanisms can reconcile theory and observations at the low-mass end of the galaxy luminos-

ity function. The role of SN feedback is uncertain since SNe might fail in a multiphase interstellar medium (ISM) (Bland-Hawthorn, Sutherland & Webster 2015). Moreover, massive dwarf galaxies seem to require stronger feedback than SNe can provide (Garrison-Kimmel et al. 2013). The role of environmental physics is also uncertain, since dwarf galaxy disagreements with the standard model seem to extend to regions where environmental effects should be small (Garrison-Kimmel et al. 2014).

X-ray observations indicate that active galactic nuclei (AGNs) are present in roughly 1 per cent of dwarf galaxies (Pardo et al. 2016; Baldassare et al. 2017), which, combined with any plausible duty cycle, suggests a larger occupation fraction for an intermediate-mass black hole (IMBH) (Miller et al. 2015). Moreover, AGN feedback could potentially provide a unified answer to dwarf galaxy issues in the standard model (Silk 2017).

In this paper, we explore the possibility of AGN feedback from an IMBH in dwarf galaxies. We compute the critical halo mass for gas expulsion out of the halo by the AGN outflow, following the example of Dekel & Silk (1986) for SNe. We examine how that critical mass depends on parameters, using standard scaling relations and a spherical model. This allows us to compare the roles of SNe and AGNs in expelling the gas. We are considering the competition between gas retention from the gravitational force of

[*] E-mail: dashyan@iap.fr

the halo and gas expulsion by the AGN. This is a different approach from the one yielding a high-mass break (Bower et al. 2006; Croton et al. 2006), which involves the role of an AGN in suppressing cooling flows on to massive galaxies, thereby modifying the bright end of the galaxy luminosity function.

In Section 2, we explain the scaling relations and the physics of the outflow driven by the AGN wind. In Section 3, we compute the critical conditions and discuss their dependence on the parameters as well as the effect of cooling. We summarize and discuss the results in Section 4.

2 MODEL

We study gas ejection from a spherical galaxy halo driven by the AGN outflow by following the propagation of the swept-up ISM (Sections 2.2 and 2.3), and comparing the outflow and local escape velocities. We use scaling relations to estimate the physical quantities (Section 2.1), with the aim of exploring the parameter space.

2.1 Scaling relations

For a given halo mass M_{halo}, the parameter space to be explored consists of the redshift, the IMBH mass, the Eddington ratio of the AGN, the fraction of mass in gas, the gas and dark matter density profiles, the velocity of the inner wind and the lifetime of the AGN. We investigate AGN feedback in early dwarf evolution, and therefore the relevant redshift is the typical redshift of halo formation, when the typical density fluctuation corresponds to a halo mass that satisfies $\sigma(M_{halo}, z) = 1$. We use a fitting function for $\sigma(M_{halo}, z)$ (appendix A of van den Bosch 2002). Therefore, the physical quantities associated to M_{halo} are computed at $z(M_{halo})$, and varying M_{halo} means varying the redshift. For a given halo mass, the virial radius R_{vir} and velocity V_{vir} are uniquely defined as

$$z = z_{nonlinear}(M_{halo}) \,, \tag{1a}$$

$$M_{halo} = \frac{4\pi}{3} \Delta_c(z) \rho_c E^2(z) R_{vir}^3 \,, \tag{1b}$$

$$V_{vir} = \sqrt{\frac{G M_{halo}}{R_{vir}}} \,, \tag{1c}$$

where G is the gravitational constant, ρ_c is the critical density of the Universe, $\Delta_c(z)$ is the density contrast relative to critical, taken from Bryan & Norman (1998), and $E^2(z) = [H(z)/H_0]^2$. We use a constant gas fraction

$$M_g = f_g M_{halo} \,, \tag{2}$$

where $f_g = \Omega_b/\Omega_m \simeq 0.17$. The dark matter and gas both follow the NFW profile of Navarro, Frenk & White (1996)

$$\rho_{DM}(r) = \frac{\rho_0}{r/R_s (1 + r/R_s)^2} \,, \tag{3a}$$

$$\rho_g = \frac{f_g}{1 - f_g} \rho_{DM} \,, \tag{3b}$$

where $R_s \approx R_{vir}/c(M_{halo}, z)$ and $c(M_{halo}, z)$ is the NFW concentration given by Dutton & Macciò (2014). The escape velocity at the virial radius is

$$V_{esc} = V_{vir} \sqrt{2 \log(1 + c)/(\log(1 + c) - c/(1 + c))} \tag{4}$$

(Cole & Lacey 1996). Using an M_{BH}–σ-type relation for the black hole (BH), we estimate the BH mass
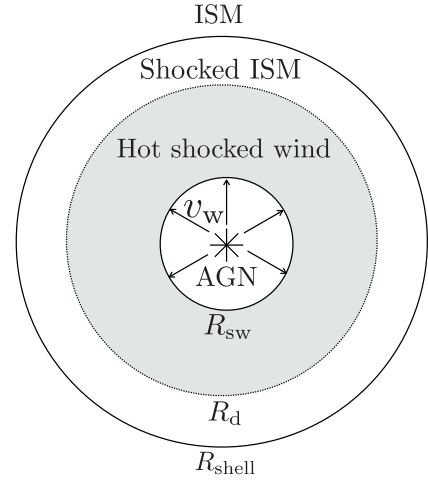
$$M_{BH} = A\sigma^\alpha \,, \tag{5}$$

Figure 1. Schematic view of the outflow structure. The accreting IMBH drives the wind with velocity v_w. It collides with the ISM and is slowed in a strong shock at R_{sw}. A forward shock, at R_{shell}, is driven into the ISM. R_d is the contact discontinuity between the shocked wind and the shocked ISM.

where the velocity dispersion $\sigma \simeq 0.7V_{vir}$ for NFW models (Łokas & Mamon 2001). We vary α between 3.5 and 5, and for each α we fit the normalization A to the observational data of Ferrarese & Merritt (2000), Gebhardt et al. (2000), Tremaine et al. (2002), Gültekin et al. (2009) and Kormendy & Ho (2013). The mechanical luminosity of the IMBH is a function of the velocity of the AGN inner wind v_w and the luminosity of the AGN, given itself by the Eddington ratio χ and the Eddington luminosity,

$$L_m = \frac{v_w}{2c} L_{AGN} = \frac{v_w}{2c} \chi L_{Eddington} = \frac{v_w}{2c} \chi \frac{4\pi G c M_{BH} m_p}{\sigma_T} \,, \tag{6}$$

where m_p is the proton mass and σ_T the Thomson cross-section. Equation (6) assumes that the outflow momentum flux is comparable to that in the emitted radiation field, L_{AGN}/c. We assume $v_w = 0.1c$, where c is the speed of light, following observations (Tombesi et al. 2010; Gofford et al. 2013; King & Pounds 2015). Finally, we define t_{AGN} as the lifetime of the AGN.

2.2 Structure of the outflow

A schematic view of the outflow structure is shown in Fig. 1. The outflow from the AGN impacts the ISM of the host galaxy, producing an inner reverse shock at R_{sw} slowing the wind, and an outer forward shock accelerating the swept-up gas at R_{shell}. A contact discontinuity separates the hot shocked wind and the shocked ISM at R_d. The shocked wind is much hotter than the shocked ISM. Therefore, the cooling of the shocked ISM has no substantial impact on the propagation. Hence, we assume, as Faucher-Giguère & Quataert (2012), that the shocked ISM is collapsed into a thin shell and define $R \equiv R_d \approx R_{shell}$. Moreover, the sound crossing time in the shocked wind is smaller than the age of the outflow and the entire region is at uniform pressure (Weaver et al. 1977).

2.3 Equations of the propagation

2.3.1 Energy-driven

The propagation is called energy-driven when no energy is lost to radiation and the energy is thereby conserved. In that case, the motion of the shell is driven by the internal energy of the shocked

wind that expands adiabatically. Following an approach similar to Weaver et al. ([1977](#)) and Koo & McKee ([1990](#)), the set of equations giving the radius of the shell and the internal energy of the gas is

$$
\begin{cases}
\frac{d}{dt}(M_{\text{shell}}(R)\dot{R}R) & 2E_{\text{th}} + M_{\text{shell}}\dot{R}^2 + E_{\text{grav,t}}, \\
E_{\text{in}} + E_{\text{grav,0}} & E_{\text{th}} + \frac{1}{2}M_{\text{shell}}\dot{R}^2 + E_{\text{grav,t}},
\end{cases} \tag{7}
$$

where M_{shell} is the mass of the gas engulfed by the blast wave at R, $E_{\text{in}}(t) = L_{\text{m}} \times \min(t, t_{\text{AGN}})$ is the total injected energy, $E_{\text{grav,0}}$ is the gravitational energy that the swept-up gas would have had in the absence of the blast wave, and $E_{\text{grav,t}}$ is the gravitational energy of the gas shell, under the gravity of the total mass engulfed by the blast wave. The first equation in (7) is the generalized virial theorem, applied to the gas engulfed by the blast wave, assuming that most of the mass is carried by the shell of a shocked ISM. The second equation simply states the conservation of energy since the propagation is adiabatic; all the input energy (E_{in}) and the initial gravitational energy ($E_{\text{grav,0}}$) at a given time during propagation go to (1) the internal energy of the shocked wind (E_{th}), (2) the kinetic energy of the shell ($\frac{1}{2}M_{\text{shell}}\dot{R}^2$) of the blast wave and (3) the current gravitational energy of the gas shell under the gravity of the total mass engulfed by the blast wave ($E_{\text{grav,t}}$).

2.3.2 Momentum-driven

The nature of the outflow depends on that of the reverse shock between the wind and the shocked wind, which in turn depends on the cooling: if the cooling is efficient, the shocked wind loses its thermal energy and compresses into a thin shell. The outflow is called momentum-driven because the shock is accelerated by the momentum input per unit time L_{AGN}/c and no longer by the adiabatic expansion of the shocked wind. The equation of propagation is

$$
\frac{d}{dt}\left[M_{\text{shell}}(R)\dot{R}\right] = \frac{L_{\text{AGN}}}{c} - \frac{GM_{\text{shell}}(R)\left[M_{\text{DM}}(<R) + M_{\text{BH}}\right]}{R^2}, \tag{8}
$$

where $M_{\text{shell}}(R)\dot{R}$ is the momentum of the shell and L_{AGN}/c is the momentum input from the photons per unit time. In the momentum-driven regime, the outflow is much less powerful than in the energy-driven regime: for an IMBH near the $M_{\text{BH}}-\sigma$ relation, only a fraction $\sim\sigma/c$ of the mechanical luminosity is transferred to the ISM (King & Pounds [2015](#)).

2.4 Energetics

The combined action of many SNe leads to the development of an expanding superbubble capable of sweeping up the ISM (Kim, Ostriker & Raileanu [2017](#)). In this section and in Section 3.2, we compare the effects of AGNs and SNe as a function of the halo mass, varying relevant parameters such as the Eddington ratio and the lifetime of the AGN. The star formation rate can be approximated as $M_{\text{SF}}/t_{\text{SF}}$, where $M_{\text{SF}} \simeq M_{\text{g}}(< R_{\text{vir}}/10)$ is the gas mass available for star formation and t_{SF} is the gas depletion time in the ISM with a redshift dependence

$$
t_{\text{SF}} = 1.26(1+z)^{-0.34}\,\text{Gyr}, \tag{9}
$$

observed by Genzel et al. ([2015](#), see their table 3). The total luminosity is

$$
L_{\text{SN}} = E_{\text{SN}}M_{\text{SF}}\nu/t_{\text{SF}}, \tag{10}
$$

where ν is the number of SNe per mass of forming stars. For a Kroupa initial mass function (Kroupa [2001](#)), $\nu = 1/100\,\text{M}_\odot$.
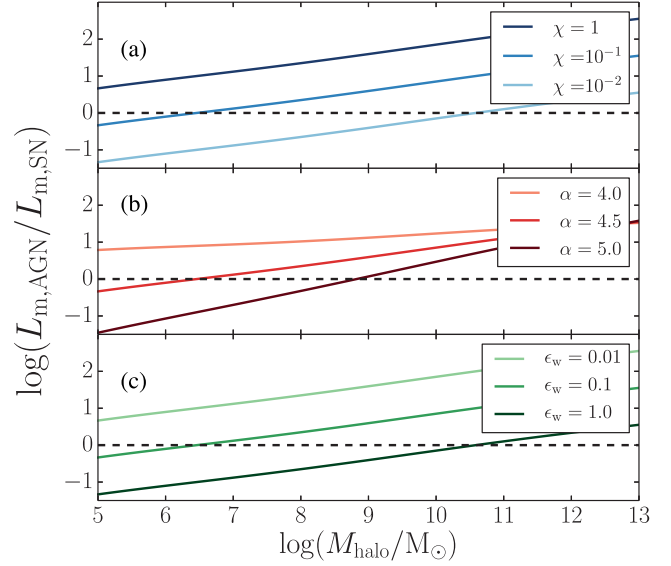

Figure 2. Ratio between the mechanical luminosity from the AGN and the mechanical luminosity from SNe, as a function of the halo mass, for different values of (a) the Eddington ratio χ, (b) the exponent α in the $M_{\text{BH}}-\sigma$ relation and (c) SNe wind efficiency ϵ_{w}. For each panel, the default values for the parameters that do not vary are $\chi = 0.1$, $\alpha = 4.5$ and $\epsilon_{\text{w}} = 0.1$.

However, only a fraction $\epsilon_{\text{w}} \sim 1$–10 per cent of L_{SN} contributes to drive an outflow (Dubois & Teyssier [2008](#)).

We compare the input wind luminosities from AGNs ($L_{\text{m, AGN}}$) and SNe ($L_{\text{m, SN}}$) through the ratio $\mathcal{R} = L_{\text{m,AGN}}/L_{\text{m,SN}}$. Fig. [2](#) shows that $\mathcal{R}$ increases with halo mass. Therefore, a halo mass exists above which the mechanical luminosity of an AGN is higher than the mechanical luminosity from SNe, and this mass depends on χ, ϵ_{w} and α. $\mathcal{R}$ increases with χ and decreases with α and ϵ_{w}. In Section 3.2, we also take into account the momentum injection by SNe, following Kim & Ostriker ([2015](#)).

In this paper, the AGN mass is uniquely defined by the halo mass and the exponent in the $M_{\text{BH}}-\sigma$ relation. By releasing that constraint, one can compute the minimum black hole mass required to energetically dominate SNe. We find

$$
\log\left(\frac{M_{\text{BH,crit}}}{\text{M}_\odot}\right) \simeq 2.8 + 1.1\log\left(\frac{M_{\text{halo}}}{10^9\text{M}_\odot}\right) + \log\left(\frac{\epsilon_{\text{w}}}{\chi}\right). \tag{11}
$$

However, this energetic approach is only of the first order because the energy cannot be considered as the deciding quantity a priori, since it can be lost through cooling processes. Therefore, it is important to use a self-consistent treatment of the cooling and to compute the propagation of the shell (see Section 3). Coupling between SNe and AGNs and geometry effects are other limitations to this simple approach, which are not addressed in this paper.

3 IMPLICATIONS

The critical condition for gas removal is that the velocity V_{shell} of the shell of a swept-up ISM is above the escape velocity when it reaches the virial radius. For both SNe and AGNs, the scaling relations are such that this critical condition defines two mass regions on both sides of the critical halo mass: for halo masses below (respectively above) the critical halo mass, the gas removal by the outflow is possible (impossible). We numerically integrate the equation of motion and compute the critical halo mass as the greatest for which the shell velocity exceeds the escape velocity at the virial radius.

For AGN- and SNe-driven shells, we use the corresponding luminosity to compute the velocity of the shell, until it reaches the virial radius or stalls. For SNe, we update the luminosity at each time-step by updating the available gas mass: we remove the amount of gas that has gone to star formation from the total available gas mass.

3.1 Cooling

If the cooling time-scale is shorter than the flow time, R_{shell}/V_{shell}, the cooling is efficient and the outflow is momentum-driven, otherwise, it is energy-driven. We include cooling processes in our model when integrating the equation of motion of the blast wave, and choose between momentum- and energy-driven accordingly. The dominant process for the cooling of the shocked wind is Compton cooling: the electrons of the shocked wind lose energy to photons via the inverse Compton effect (Ciotti & Ostriker 1997; Hartwig, Volonteri & Dashyan 2017). The Compton cooling time is given by

$$t_C = \frac{3m_e c}{8\pi\sigma_T U_{rad}} \frac{m_e c^2}{E} , \qquad (12)$$

where m_e is the mass of an electron, $E = 9m_p v_w^2/16$ is the energy of an electron in the shocked wind and $U_{rad} = L_{AGN}/(4\pi R_{sw}^2 c)$ is the radiation density in the wind. At the beginning of the outflow, close to the IMBH, the radiation field is intense enough to cool the shocked wind: the outflow starts momentum-driven and $t_C \propto R^2$. Integrating equation (8), the flow time in the momentum-driven regime follows $t_{flow} \propto R^{2+s/2}$, where $s < -1$ is the local slope of the NFW profile. Comparing the scaling of $t_C(R)$ and $t_{flow}(R)$, one sees that while gravity is negligible and as long as the AGN shines, a radius of transition to an energy-driven expansion exists.

To compute the effect of other cooling mechanisms, we use the Sutherland & Dopita (1993) cooling function approximated in a polynomial form by Tozzi & Norman (2001). We find that subsequent radiative cooling becomes important only once the shell has slowed down to velocities much lower than the escape velocity and therefore has a negligible influence on the fate of the swept-up gas (see also Hartwig et al. 2017).

Fig. 3 displays the propagation for different (χ, t_{AGN}) pairs. The critical mass is the halo mass (1) below which the shell velocity is above the escape velocity at the virial radius and (2) above which the shell slows down before reaching the virial radius because of the inertia of the swept-up gas, gravity and/or cooling. The transition from the initial momentum- to energy-driven is visible in the upper right-hand panel: it corresponds to the abrupt early rise of the velocity of the bottom curve. For each panel, one can see a break in the velocity curve (e.g. at $t = t_{AGN} = 1$ Myr in the upper right-hand panel), when the AGN stops shining. The smooth reacceleration of the shell, visible in the top curve of the lower right-hand panel, is due to the increasingly steeper slope of the NFW profile: beyond the scale radius, the gas is so tenuous that the shell can reaccelerate. Note that we do not consider two-temperature effects (Faucher-Giguère & Quataert 2012), which increases the Compton cooling time and thus leads to an earlier transition to adiabatic expansion, and therefore enhances gas ejection.

3.2 Parameter study

Fig. 4 shows the critical halo mass: for each pair of parameters (t_{AGN}, χ) (panel a) and (t_{AGN}, α) (panel b), we compute the critical halo mass below which gas removal by the AGN is possible, i.e. for which $V_{shell}(R_{vir}) > V_{esc}(R_{vir})$. White dashed contours indicate $M_{crit} = 10^8$,
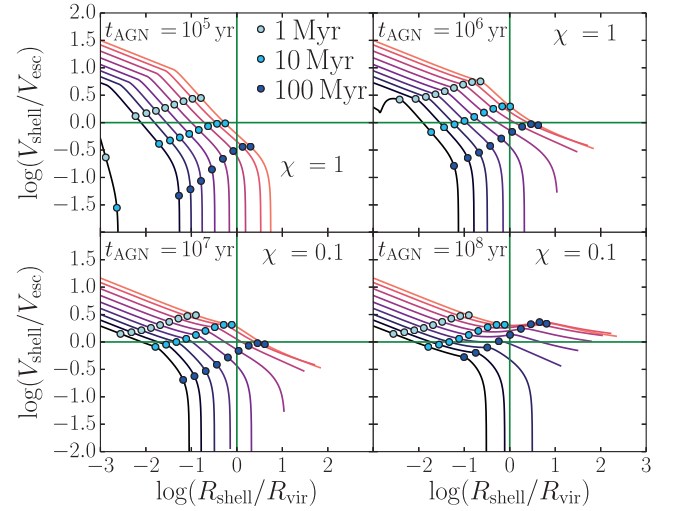

Figure 3. Velocity of the shell (normalized to the escape velocity at the virial radius) as a function of the radius of the shell (normalized to the virial radius), for different halo masses – from $M_{halo} = 10^5 \, M_\odot$ (top curve in each panel) up to $M_{halo} = 10^{13} \, M_\odot$ (bottom curve in each panel), with all the integer powers of 10 in between. We assume an exponent $\alpha = 4$ in the M_{BH}–σ relation. The time markers give the propagation time after 1, 10 and 100 Myr. We show the propagation for four pairs (χ, t_{AGN}). The critical halo mass is the greatest for which gas removal is possible, i.e. $V_{shell}(R_{vir}) > V_{esc}(R_{vir})$.

10^{10} and $10^{12} \, M_\odot$. In panel (a), the critical mass increases towards the upper right corner of the panel. Therefore, for a given halo mass, gas removal is possible for the parameters (t_{AGN}, χ) that are on the upper right side of the corresponding white dashed contours. Similarly, in panel (b), the critical halo mass increases towards the lower right side of the panel. Black dash–dotted contours show where the critical halo masses for AGNs and SNe are equal for given values of ϵ_w (0.1 and 1). Note that the critical mass for SNe, at a given value of ϵ_w, is constant over these plots. Since a higher critical halo mass indicates stronger feedback, these contours also split the parameter space into two regions: in panel (a), AGN feedback dominates SN feedback on the upper right side of the black contours and SN feedback dominates AGN feedback on the lower left side, and in panel (b) AGNs dominate on the lower right side of the black contours and vice-versa. AGN feedback is greater than SNe feedback in a significant part of the parameter space, since Dubois & Teyssier (2008) compute values of ϵ_w smaller than 10 per cent.

In panel (a) of Fig. 4, one sees that the contour plots for low halo masses follow straight lines with a slope of -1. This occurs because the outflow is mostly energy-driven for masses below the critical halo mass: what mostly counts is the input energy, i.e. $L_m t_{AGN}$, which is constant along the lines of slope -1. However, the critical halo mass does not depend on t_{AGN} above a certain value of t_{AGN}. The reason is that the energy needs to be applied on a time-scale shorter than the free-fall time of the galaxy in order to overcome gravity. Regarding the comparison with SNe feedback, given a halo mass, and a value of ϵ_w, the SN luminosity is uniquely defined, which means that for parameters along the contours where $M_{crit, SN} = M_{crit, AGN}$, the luminosity for SNe is uniform (e.g. $L_{SN} = 3 \times 10^{40}$ erg, for $\epsilon_w = 1$), whereas the AGN kinetic luminosity varies, and yet the critical mass is the same. The reason is that we turn off the AGN after t_{AGN}, but do not turn off SN kinetic power. Therefore, input energy and kinetic luminosities are good first-order approaches but
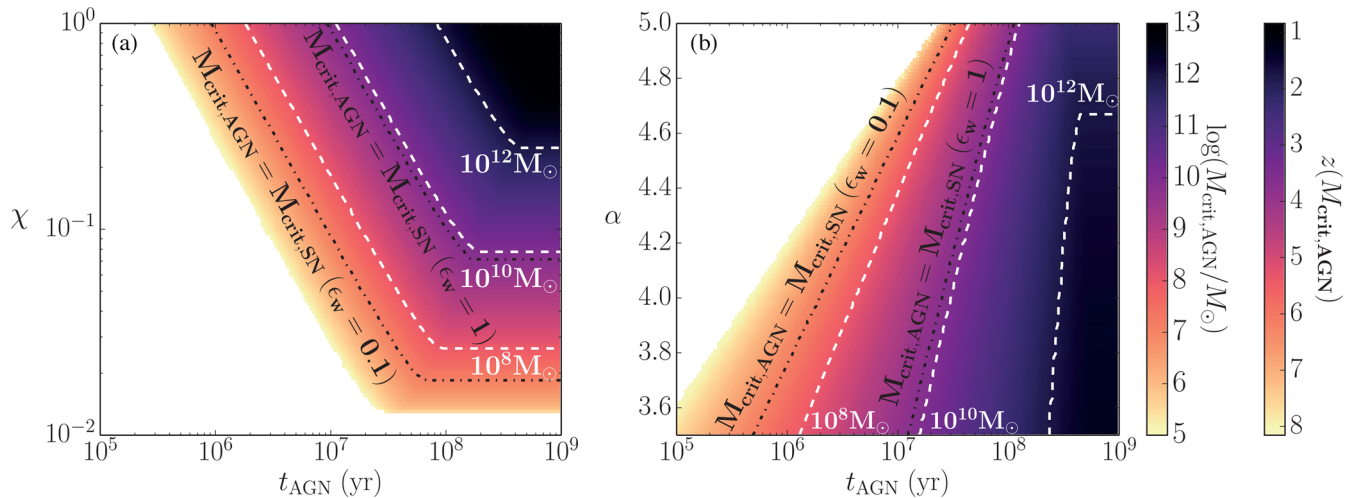
Figure 4. Critical halo mass below which gas removal by the AGN is possible, i.e. $V_{shell}(R_{vir}) > V_{esc}(R_{vir})$, (a) as a function of the Eddington ratio χ and t_{AGN}, with the slope of the M_{BH}–σ relation $\alpha = 4$ and (b) as a function of α and t_{AGN}, with $\chi = 0.3$. We show in a second colour bar the corresponding redshift according to equation (1a). White dashed contours indicate $M_{crit} = 10^8$, 10^{10} and 10^{12} M$_\odot$. In panel (a), the critical mass increases towards the upper right corner of the panel. Therefore, for a given halo mass, gas removal is possible for the parameters (t_{AGN}, χ) that are on the upper right side of the corresponding white dashed contours. Similarly, in panel (b), the critical halo mass increases towards the lower right side of the panel. Black dash–dotted contours show where the critical halo masses for AGNs and SNe are equal. Note that the critical mass for SNe, at a given value of ϵ_w, is constant over these plots. Since a higher critical halo mass indicates stronger feedback, black contours also split the parameter space into two regions: in panel (a), AGN feedback dominates SN feedback in areas on the upper right side of the black contours and vice versa and in panel (b) AGNs dominate in areas on the lower right side of the black contours and vice versa. AGN feedback is greater than SNe feedback in a significant part of the parameter space.

one has to consider the time-scales during which the energies are applied.

In panel (b), one sees that the contour plots are closer for higher values of α, which means that the dependence of the critical halo mass as a function of t_{AGN} at fixed α is steeper for higher values of α. The reason is that the ratio E_{input}/E_{grav}, which quantifies to the first order the effect of the AGN on the galaxy, is a shallower function of M_{halo} for higher values of α, for which the value of the critical halo mass is more sensitive to the normalization of that ratio, and thus to t_{AGN}. Note that when computing the expansion of the SN wind, we do not consider the cooling of the hot interior of the bubble, which, if significant, should lower the critical halo mass for SNe and thus widen the subspace of an AGN predominance.

In the manner of equation (11), we can release the constraint on the black hole mass given by the M_{BH}–σ relation and compute, using the equation of motion, the critical black hole mass above which AGN feedback is stronger than SN feedback. Fig. 5 shows the critical black hole mass above which the AGN-driven shell is pushed further in the ISM than the SN-driven shell, as a function of the halo mass, for a given set of parameters (t_{AGN}, ϵ_w, χ). One sees that the scalings found energetically in equation (11) and by solving the equation of motion of motion of the shell are similar. We retrieve the linear dependence of the critical black hole mass on ϵ_w/χ, computed energetically in equation (11). However, in the upper panel, the influence of the duration of the AGN can be seen with the sharp rise in the critical BH-to-halo mass relation, which does not appear in equation (11). This rise, for $t_{AGN} = 10^5$ and 10^6 yr, indicates that the transition to an energy-driven propagation occurs later for higher black hole masses, and, hence, that transition never occurs for short t_{AGN} and high black hole masses.

4 DISCUSSION AND CONCLUSION

In this paper, we investigated the possibility of AGN feedback in dwarf galaxies. Assuming scaling relations between the relevant
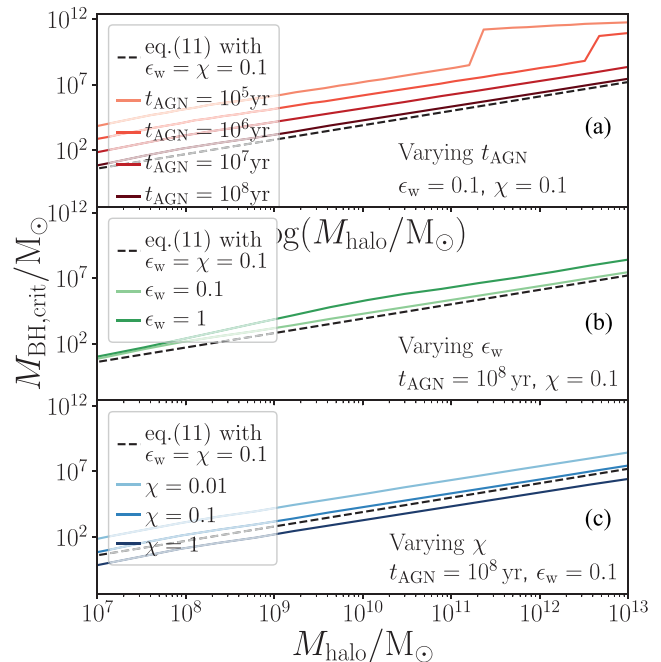

Figure 5. Critical black hole mass above which, for a given halo mass, AGN feedback is stronger than SN feedback for different values of (a) the duration of the AGN, t_{AGN}, (b) the SN wind efficiency ϵ_w and (c) the Eddington ratio χ. The black dashed line indicates the scaling found energetically in equation (11). The scalings found energetically and by solving the equation of motion of motion of the shell are similar except for the short AGN time durations ($t_{AGN} = 10^5$ and 10^6 yr) for which the sharp rise reveals the transition from an energy-driven to a momentum-driven only AGN outflow.

physical quantities, we obtained a critical halo mass below which gas removal by the AGN is possible. In a broad part of the parameter space, AGN feedback is more efficient than SNe feedback. This suggests that an AGN could succeed where SNe might fail, such as in the most massive dwarf galaxies. We argue that an AGN could potentially have played a significant role in gas ejection in early dwarf evolution.

In our definition, AGN feedback is *efficient* when the AGN-driven shell escapes the virial radius of the galaxy. This does not mean that AGN feedback is not efficient at regulating star formation in massive haloes, just that there are no escaping winds. In particular, we do not include the effect of AGN feedback on the accretion of cooling flows. Moreover, in high-redshift small-mass disc galaxies, the effect of an AGN should be smaller than in our 1D model because the outflow can escape in the perpendicular direction as analysed by Hartwig et al. (2017). Besides, our work does not address the interplay between SN and AGN feedback: efficient SN feedback can prevent the accumulation of dense cold gas and starve the black hole (Dubois et al. 2015). A full treatment of this phenomenon would constrain the explorable parameter space for the black hole and minimize the predominance of an AGN. A complete treatment would also include a multiphase ISM, which, when taken into consideration, reduces the feedback efficiency for both AGNs (Costa, Sijacki & Haehnelt 2014) and SNe (Bland-Hawthorn et al. 2015). An AGN can also trigger star formation as proposed theoretically (Silk & Norman 2009; Gaibler et al. 2012) and seen observationally (Maiolino et al. 2017). More realistic simulations, including much of this additional physics, are needed before we can fully understand the role of AGN feedback in the multiphase ISM of initially gas-rich dwarf galaxies.

ACKNOWLEDGEMENTS

REFERENCES

Baldassare V. F., Reines A. E., Gallo E., Greene J. E., 2017, ApJ, 836, 20
Bland-Hawthorn J., Sutherland R., Webster D., 2015, ApJ, 807, 154
Bower R. G., Benson A. J., Malbon R., Helly J. C., Frenk C. S., Baugh C. M., Cole S., Lacey C. G., 2006, MNRAS, 370, 645
Boylan-Kolchin M., Bullock J. S., Kaplinghat M., 2011, MNRAS, 415, L40
Bryan G. L., Norman M. L., 1998, ApJ, 495, 80
Ciotti L., Ostriker J. P., 1997, ApJ, 487, L105
Cole S., Lacey C., 1996, MNRAS, 281, 716
Costa T., Sijacki D., Haehnelt M. G., 2014, MNRAS, 444, 2355
Croton D. J. et al., 2006, MNRAS, 365, 11
Dekel A., Silk J., 1986, ApJ, 303, 39
Dubois Y., Teyssier R., 2008, A&A, 477, 79
Dubois Y., Volonteri M., Silk J., Devriendt J., Slyz A., Teyssier R., 2015, MNRAS, 452, 1502
Dutton A. A., Macciò A. V., 2014, MNRAS, 441, 3359
Faucher-Giguère C.-A., Quataert E., 2012, MNRAS, 425, 605
Ferrarese L., Merritt D., 2000, ApJ, 539, L9
Gaibler V., Khochfar S., Krause M., Silk J., 2012, MNRAS, 425, 438
Garrison-Kimmel S., Rocha M., Boylan-Kolchin M., Bullock J. S., Lally J., 2013, MNRAS, 433, 3539
Garrison-Kimmel S., Boylan-Kolchin M., Bullock J. S., Kirby E. N., 2014, MNRAS, 444, 222
Gebhardt K. et al., 2000, ApJ, 539, L13
Genzel R. et al., 2015, ApJ, 800, 20
Gofford J., Reeves J. N., Tombesi F., Braito V., Turner T. J., Miller L., Cappi M., 2013, MNRAS, 430, 60
Gültekin K. et al., 2009, ApJ, 698, 198
Hartwig T., Volonteri M., Dashyan G., 2017, MNRAS, preprint (arXiv:1707.03826)
Kim C.-G., Ostriker E. C., 2015, ApJ, 802, 99
Kim C.-G., Ostriker E. C., Raileanu R., 2017, ApJ, 834, 25
King A., Pounds K., 2015, ARA&A, 53, 115
Koo B.-C., McKee C. F., 1990, ApJ, 354, 513
Kormendy J., Ho L. C., 2013, ARA&A, 51, 511
Kroupa P., 2001, MNRAS, 322, 231
Łokas E. L., Mamon G. A., 2001, MNRAS, 321, 155
Maiolino R. et al., 2017, Nature, 544, 202
Miller B. P., Gallo E., Greene J. E., Kelly B. C., Treu T., Woo J.-H., Baldassare V., 2015, ApJ, 799, 98
Moore B., Ghigna S., Governato F., Lake G., Quinn T., Stadel J., Tozzi P., 1999, ApJ, 524, L19
Navarro J. F., Frenk C. S., White S. D. M., 1996, ApJ, 462, 563
Oh S.-H., Brook C., Governato F., Brinks E., Mayer L., de Blok W. J. G., Brooks A., Walter F., 2011, AJ, 142, 24
Pardo K. et al., 2016, ApJ, 831, 203
Silk J., 2017, ApJ, 839, L13
Silk J., Norman C., 2009, ApJ, 700, 262
Sutherland R. S., Dopita M. A., 1993, ApJS, 88, 253
Tombesi F., Cappi M., Reeves J. N., Palumbo G. G. C., Yaqoob T., Braito V., Dadina M., 2010, A&A, 521, A57
Tozzi P., Norman C., 2001, ApJ, 546, 63
Tremaine S. et al., 2002, ApJ, 574, 740
van den Bosch F. C., 2002, MNRAS, 331, 98
Weaver R., McCray R., Castor J., Shapiro P., Moore R., 1977, ApJ, 218, 377

This paper has been typeset from a TEX/LATEX file prepared by the author.